Chapter – 8

Effect of Cr^{3+}-doping on crystalline perfection and optical properties of ZTS: The NLO single crystals

Abstract

An interesting study of the effect of Cr^{3+}-doping in tris(thiourea)zinc sulphate single crystal on crystalline perfection and optical properties has been carried out. Pure and chromium (1 and 2 mol %) doped ZTS single crystals were grown by slow evaporation solution technique. The actual concentration of chromium incorporated into the crystal lattice was evaluated by flame atomic absorption spectroscopy. The high-resolution X-ray diffraction analysis revealed that the chromium doping lead to the creation of vacancies in the doped crystals. The photoluminescence emission also used for the defects analysis. The optical transparency in entire visible region decreased but band gap increased with doping. The wavelength dispersion, optical dielectric constant (ε), extinction coefficient (k), average single oscillator energy for electronic transitions (E_o) and the oscillator strength (E_d) have been evaluated using the ellipsometry.

8.1 INTRODUCTION

As described in the earlier chapters tris(thiourea)zinc sulphate (ZTS) is very strategic material which can be easily grown by slow evaporation solution technique. The physical properties of it in pure as well as in doped form have been well studied. The transition metal ions greatly influence the optical properties of the crystals specially by bringing the significant change in the refractive index. The dispersion behaviour of NLO single crystals has been studied and found to be significantly influenced by the metal ions (Wong 2002). The Zn, Mg, In are said to photoexhibitors lead to the enhancement of second harmonic generation and optical transparency of single crystals, whereas, Fe, Co, Cr, Cu, *etc.* are defined as photoinhibitors and later help to improve the photorefractive behaviour of single crystals.

Cadmium doping lead to high laser damage threshold and wide optical transparency of ZTS and better optical properties were obtained by mixing of phosphate groups (Venkataramanan *et al.,* 1995; Ushasree, Jayavel *et al.,* 1999). Our recent studies on ZTS in the presence of some inorganic/organic dopants elucidated the enhancement of crystalline perfection which in turn leads to the improvement in the SHG efficiency (Bhagavannarayana *et al.,* 2006; 2008). In spite of available many studies about the dopants and physical properties on ZTS single crystals there is a wide scope to investigate the minute changes in the lattice structure of the single crystals with dopants and discover the possible correlation between the physical properties of single crystals with changes in the crystal lattice. The dopants are expected to enhance some properties, but at the same time above a critical dopant concentration they may deteriorate the properties. At higher concentrations, due to stresses, the dopants may cause grain boundaries, so it is advisable that crystals must be free from the structural grain boundaries (Bhagavannarayana, Budakoti *et al.,* 2005) by keeping the dopant concentration at moderate values. Like other photoinhibitors chromium is a photorefractive element and therefore modifies the optical parameters of single crystals significantly by modifying their refractive indices (Chah *et al.,* 1997; Deanna *et al.,* 1998). It has been used to improve the photorefraction efficiency (Yasuo Tomita at al. 1993; Neurgaonkar *et al.,* 1989; Yeh *et al.,* 1994) suitable for holographic applications.

In the present investigation, for the first time, the effect of chromium (a photorefractive candidate) doping on the optical properties on ZTS single crystals has been studied. The single crystals of pure and Cr-doped ZTS were grown in pure and 1 and 2 mol% chromium added saturated aqueous solutions by slow evaporation solution technique (SEST). The actual concentration of chromium in doped ZTS crystals has been determined by flame atomic absorption spectroscopy (AAS). The crystalline perfection of undoped and doped crystals has been evaluated by high resolution X-ray diffractometry (HRXRD). Photoluminescence (PL) emission behaviour of the crystals was analyzed to visualize the formation of colour centres revealed by the vacancies observed by HRXRD. The transparency, absorption coefficient and optical band gap measurements were carried out. The wavelength dependent refractive index (wavelength dispersion) and optical dielectric characterizations were performed by employing the ellipsometry.

8.2 CRYSTAL GROWTH

The single crystals of pure and chromium doped ZTS were successfully grown by slow evaporation solution technique (Bhagavannarayana & Kushwaha, 2010) [§2.2.4]. For the growth of doped crystals the required amount of chromium chloride as per 1.0 and 2.0 mol% doping was added during the preparation of saturated solutions of ZTS. The continuous stirring was applied during solution preparation and the crystal growth was performed at a constant temperature 300 k in a constant temperature bath. The good quality single crystals were harvested from the mother solutions after a span of 20 days and their photographs are shown in Fig. 8.1. From photographs it can be clearly seen that the pure and 1 mol% doped crystals are quite transparent, whereas 2 mol% doped crystal is slightly opaque having whitish structure inside. The low visual transparency of 2 mol% doped crystal may be attributed to the presence of high concentration of vacancies, which are well explained in the forthcoming HRXRD section.

8.3 CHARACTERIZATION STUDIES

The crystal structure and unit cell parameters of the grown crystals were analyzed using a Bruker AXS D8 Advanced powder X-ray diffractometer (PXRD)

with CuK_{α} radiation having graphite monochromator. The diffraction spectra of the fine powdered specimens of pure as well as doped crystals were recorded in the two-theta range of 10–80 degrees. The actual concentration of Cr incorporated into the crystal lattice was determined by atomic absorption spectroscopy (AAS) (Analytik Jena, Vario-6) [§3.1] with a vapour generation accessory (AAS-HG). Known amount of crystal specimens were dissolved in de-ionized water and subjected to analysis.

The PANalytical X'Pert PRO MRD, high resolution X-ray diffraction system, having $CuK\alpha_1$ radiation, was employed to assess the crystalline perfection of pure and doped crystals. The fine monochromated X-ray beam ($CuK\alpha_1$) was obtained by using a hybrid 2-bounce Ge(220) monochromator with parabolic multilayer mirror assembly. The rocking curves of crystals for (200) diffraction planes were recorded in symmetrical Bragg geometry using by performing ω-scan with triple axis geometry [§3.3].

The room-temperature PL emission spectra of the crystal were recorded using a Perkin Elmer LS-55 Luminescence Spectrometer in the wavelength range of 400-700 nm at the room temperature. The area of the crystal surfaces exposed to the incident beam was kept constant for all the specimens. A cut-off filter of 390 nm was used to separate out the wavelength of excitation from the emission spectra reaching the photomultiplier tube (detector) [§3.11]. The UV-VIS-NIR transmission and absorption measurements were carried out on Shimadzu 1601 spectrophotometer in the 200 – 1100 nm wavelength range. The well-polished specimen crystals with same thickness were subjected to the studies. To evaluate the wavelength dispersion behaviour, extinction coefficient and optical dielectric constants of pure and doped ZTS single crystals were studied by the ellipsometry in wavelength range of 245-1000 nm. The data were recorded for the (100) surfaces [§3.9].

8.4 RESULTS AND DISCUSSION

8.4.1 Atomic absorption spectroscopic and powder X-ray diffraction analysis

The concentration of chromium in doped crystals was evaluated with respect to the elemental composition of pure ZTS. The actual calculated amount of Cr found

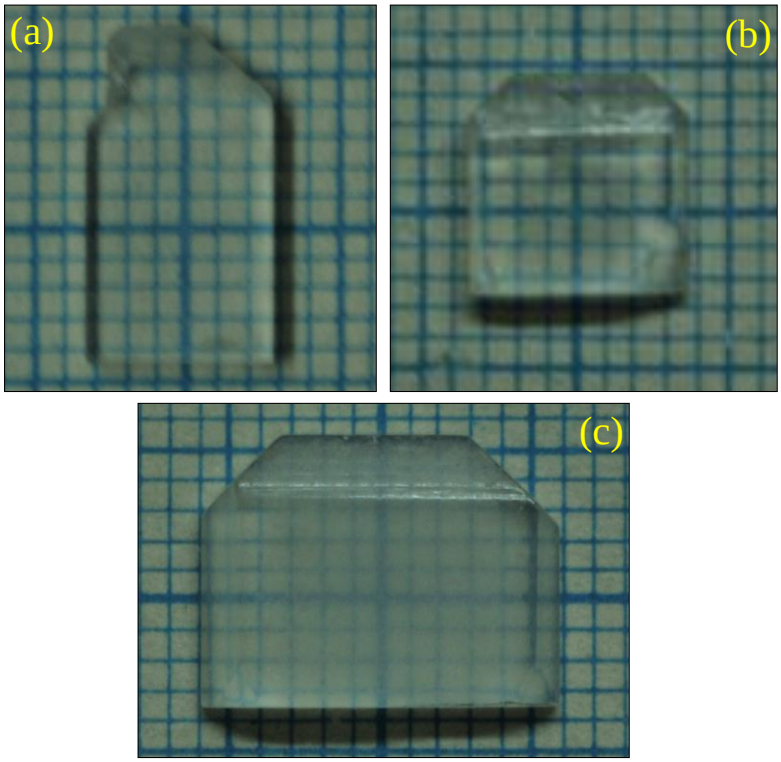

Fig. 8.1: *The photographs of SEST grown (a) pure, (b) 1 mol% and (c) 2 mol% Cr doped ZTS single crystals*

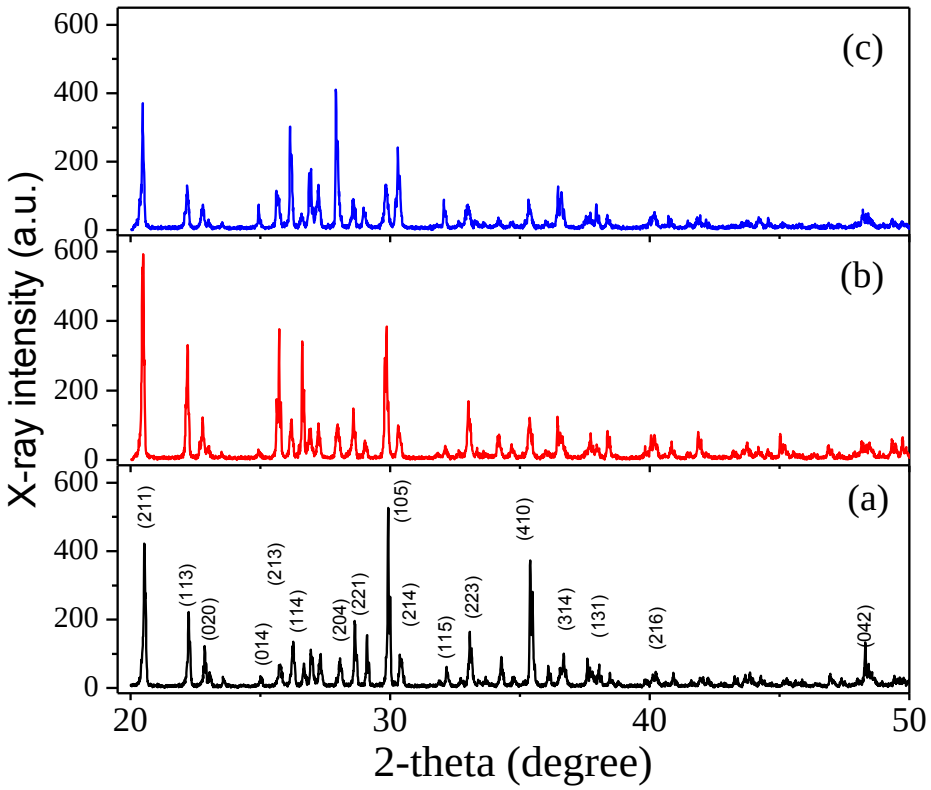

Fig. 8.2: *The PXRD spectra of (a) pure and (b) 1 mol% and (c) 2 mol% Cr^{3+} doped ZTS crystals*

in the doped single crystals is very less than the concentration of Cr added in the solution during the growth process. For 1 and 2 mol% doping the actual incorporated amount of Cr was found to be 45 and 55 ppm respectively. The powder XRD analysis confirmed the orthorhombic crystal system and space group (Pca2_1 (point group mm2)) of the grown crystals and no extra phase was observed in the doped crystals (Andreettie *et al.,* 1968), the diffraction spectra of the crystals are shown in Fig. 8.2. The calculated lattice parameters of the crystals were found to be consistent with earlier reported (Andreettie *et al.,* 1968) and insignificant variation was observed for doped crystals.

8.4.2 High resolution X-ray diffraction analysis

The recorded HRXRD rocking curves (RCs) for (200) diffraction planes of the pure, 1 mol% and 2 mol% Cr^{3+} doped single crystal specimens are shown respectively in Figs. 8.3(*a*), (*b*) and (*c*). The exact diffraction peak position is taken as zero for all the specimens. In all the RCs, no normalization was made for diffracted intensity. All the three RCs have single peak, which exhibit that the grown crystals are free from the structural grain boundaries (Bhagavannarayana, Ananthamurthy *et al.*, 2005). The RC of the pure crystal [Fig. 8.3(*a*)] is very sharp and its FWHM (full width at half maximum) is 11 arcsec which is fairly low and close to that of expected for an ideally perfect single crystal according to the plane wave dynamical theory of X-ray diffraction (Batterman *et al.*, 1964). The sharp rise and fall of the diffracted intensity on the both sides of Bragg's peak position depicts that the crystals have very low density of point defects and their agglomerates (Lal & Bhagavannarayana, 1989). However on close observation of RC of pure crystal one can see that with respect to the zero peak position, the scattered intensity in the –ve side is slightly higher in comparison to that of +ve side. Such asymmetry of RC depicts that the pure crystal contains vacancy type of defects.

This can be well understood from the fact that the lattice around the vacancy defect undergoes the expansion and lead to increase of the lattice parameter d, which results in higher scattering intensity at the lower angles with respect to the exact peak position, according to Bragg's condition ($2d\sin\theta_B = n\lambda$, where d is the lattice parameter and λ is the wavelength of incident X-ray beam).

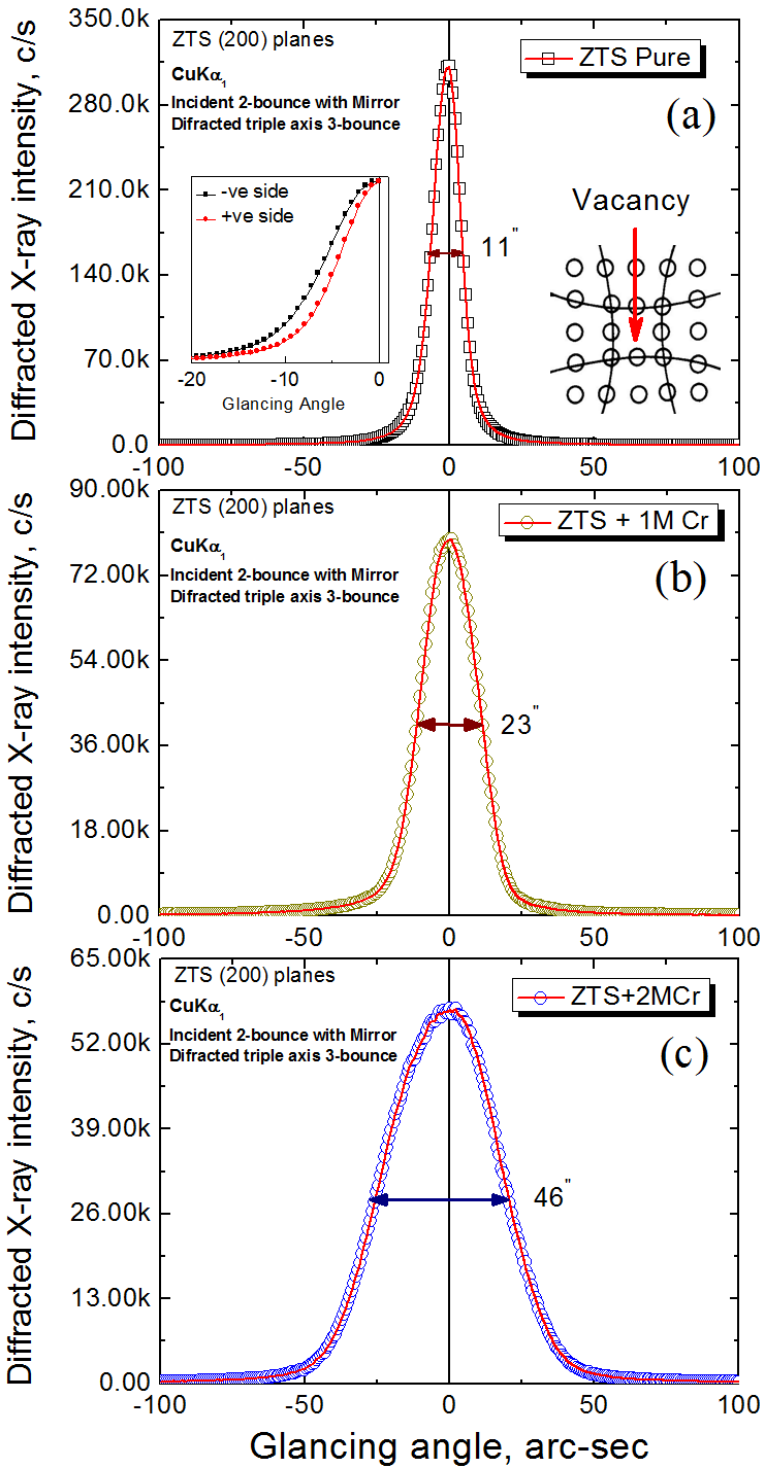

Fig. 8.3: *The high resolution X-ray Diffraction curves recorded for (200) diffraction planes of (a) pure, (b) 1 mol% and (c) 2 mol% Cr^{3+} doped ZTS single crystals*

The inset of Fig. 8.3(*a*) shows the schematic of lattice expansion towards the centre of the vacancy but only around the defect core. The RC for 1 mol% doped crystal [Fig. 8.3(*b*)] is quite broader in comparison to that of pure crystal.

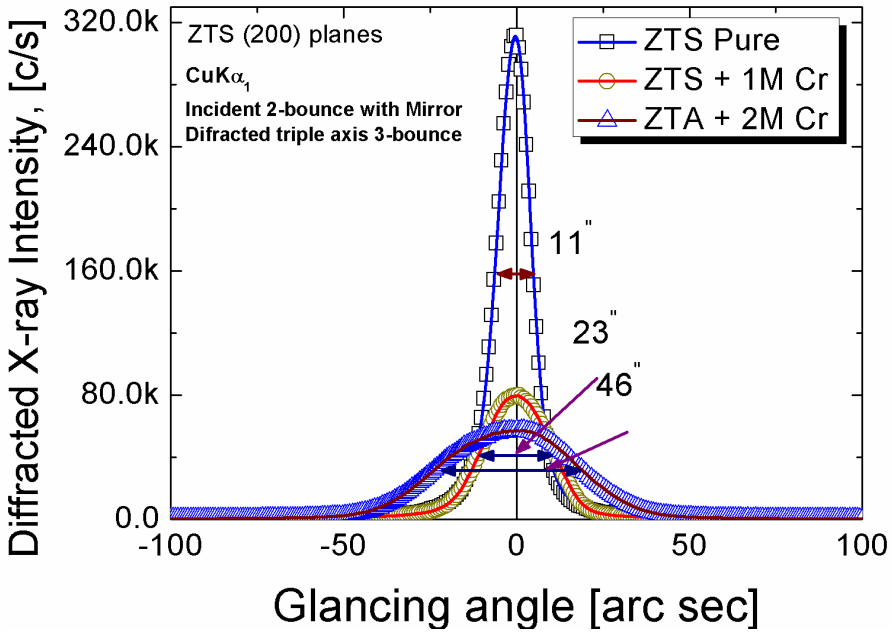

Fig. 8.4: *The high resolution X-ray Diffraction curves of the pure and doped ZTS single crystals (Fig. 7.3) plotted on a common scale of glancing angle*

With doping, the FWHM of the RC increased significantly, *i.e.* from 11 to 23 arcsec without having any significant asymmetry which indicates that the doped crystal contains both vacancy as well as interstitial point defects. The increase in FWHM of the curve may be attributed to the incorporation of chromium in ZTS crystal lattice. When the doping concentration is increased (2 mol%), the FWHM of RC further increased to 46 arcsec [Fig. 8.3(c)]. As seen in the figure, one can see a clear asymmetry in the diffracted intensity with respect to the peak position. This asymmetry in the curve with higher scattered intensity in the –ve side of the peak position clearly indicates the presence of vacancies predominantly in the crystal which may be generated due to the incorporation of Cr in Cr^{3+} ionic state at the substitutional sites of Zn^{2+}. Chromium in general exists in trivalent state. The ionic radius of Zn^{2+} is 88 pm and that of Cr^{2+} and Cr^{3+} are respectively 90 and 75.5 pm. These values indicate the easy accommodation of Cr^{3+} than that of Cr^{2+} and hence the probability of substitutional occupation of Cr^{3+} is further confirmed.

However, due to charge neutrality, Cr^{3+} doping in crystals leads to the formation of vacancies (Haixuan *at al.*, 2009; Sambasiva *et al.*, 1980; Meierling *et. al.*, 1971; Ralf *et al.*, 2009). Although the FWHM of curve for 2 mol% doping increased almost four times to that of pure crystal, the absence of extra peak indicates

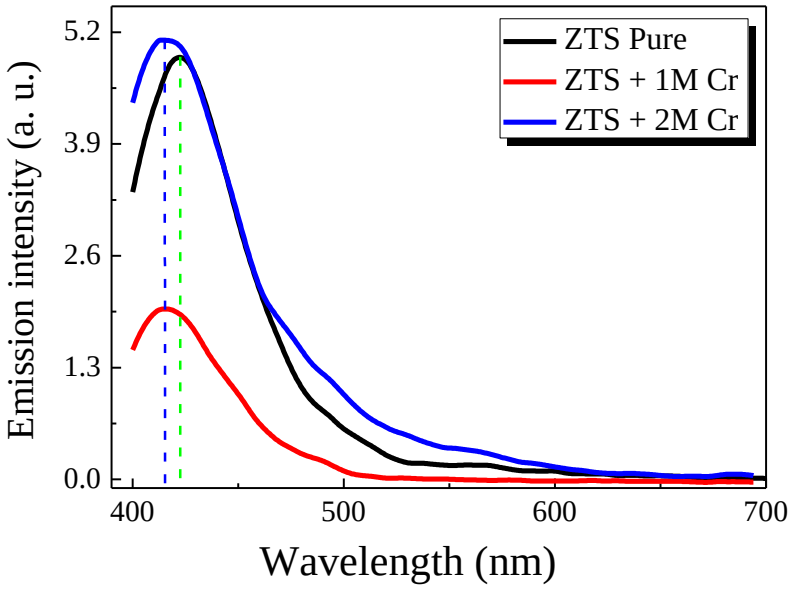

Fig. 8.5: *The photoluminescence emission spectra for pure, 1 mol% and 2 mol% Cr-doped ZTS single crystals*

that Cr^{3+}-dopants have been properly accommodated in the host ZTS lattice without leading to any structural grain boundaries. For more clarity of variation in diffracted X-ray intensity or FWHM variation with doping, the RCs for all the three specimens have been plotted together as given in Fig. 8.4. One interesting point in all the curves is that the integrated intensity (i.e. the area under the curves) is more or less same for all the curves which indicate the incorporation of dopants uniformly in the crystal.

8.4.3 Photoluminescence analysis

The recorded PL emission spectra for pure and doped ZTS crystals are shown in Fig. 8.5. The excitation wavelength for which emission spectra have been recorded is 358 nm. The pure crystal shows strong blue emission peaking at 423 nm of the electromagnetic spectrum. This is attributed to the intrinsic vacancy defects developed in the pure crystals (Xu *et. al.*, 1998; Pankratov *et al.*, 2007), which is in agreement with the HRXRD results. With the doping of Cr^{3+} ions (1 mol%) to the ZTS crystal, initially the PL intensity quenched drastically due to the "poisoning effect" as observed in other ions such as Fe, Co, Ni, *etc.* (Borse *et al.*, 1999; Rodriguez *et al.*, 2007). In other words, the radiationless redistribution of excitation energy takes place via interaction between the emitting centers and the quenching ions. However, if the doping concentration is increased to 2 mol%, it has been observed that the vacancy

related defects (F-centers) increased predominantly which act as color centers and lead the crystal to regain the PL intensity. It is in tune with the observed HRXRD results which revealed that vacancy defects are considerably very high (Haixuan *et al.*, 2009) due to the charge compensation mechanism, in 2 mol% doped sample. The enhanced vacancy concentration lead to considerable enhancement in PL intensity as observed in LiF crystals grown with vacancies (Bhagavannarayana, Kushwaha *et al.*, 2010). Interestingly, a slight shift in the PL peak position is observed towards the shorter wavelengths upon Cr^{3+} doping in ZTS crystals, which is anomalous in nature.

8.4.4 UV-VIS-NIR analysis

The recorded transmission spectra for the pure and doped single crystal specimens are shown in Fig. 8.6. The spectrum of pure crystal indicates that it has good transparency in the entire visible region right from 300 nm. The transparency of crystals reduced significantly with the doping of Cr^{3+}. The slight decrease in transparency in 1 mol% Cr-doped specimen and heavy decrease in 2 mol% Cr doped specimen may be attributed to the existence of the broad absorption band in the visible region due to Cr^{3+} dopants (Rajeev *et al.*, 2003), which lead to the formation of vacancies as revealed by HRXRD. The vacancies in crystal generally act as the photon trapping centres and absorb the light radiation and hence lead to the poor transparency (Bhagavannarayana, Kushwaha *et al.*, 2010). In spite of the decrease in transparency in the visible region, the doped crystals exhibit the enhancement in the transparency range towards the lower wavelengths compared to that of pure crystal. The absorption coefficients (α) *vs.* wavelength plots are shown in Fig. 8.7(*a*). The blue shift in the cut off wavelength of ~20 nm has been observed for the doped crystals as can be seen with clarity in the inset of figure. Though the value of α in the UV-region is lesser for doped crystals than that of pure crystal, it is higher in the entire visible region. The optical band gaps of the pure and doped crystals are evaluated by using the relation: $(\alpha h\nu)^2 = A(E_g - h\nu)$ and the plots of $(\alpha h\upsilon)^2$ *vs.* $h\upsilon$ [Fig. 8.7(*b*)], where, E_g represents the optical band gap and A is a constant (Ilashchuk *et al.*, 2010).

The E_g has been evaluated by extrapolating the linear part of the plots to abscissa (hυ) as shown in figure.

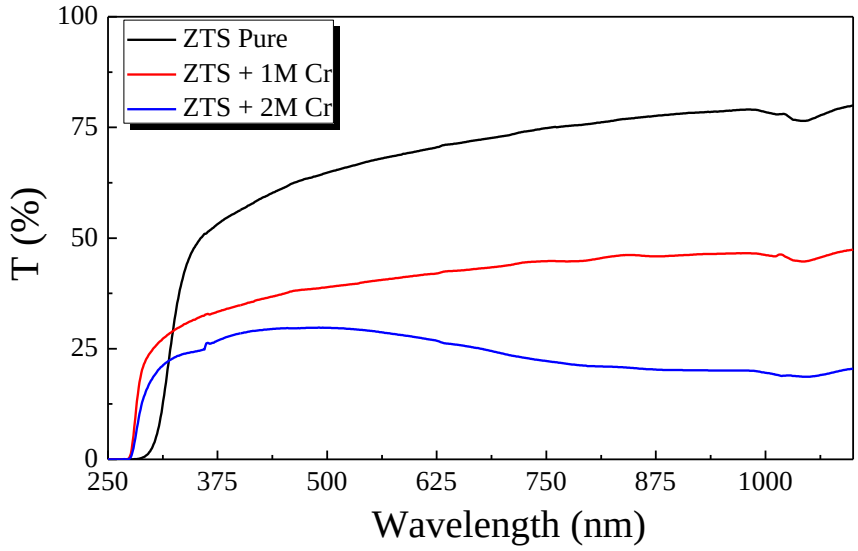

Fig. 8.6: *The optical transparency spectra for pure, 1 mol%, and 2 mol% Cr-doped ZTS crystals*

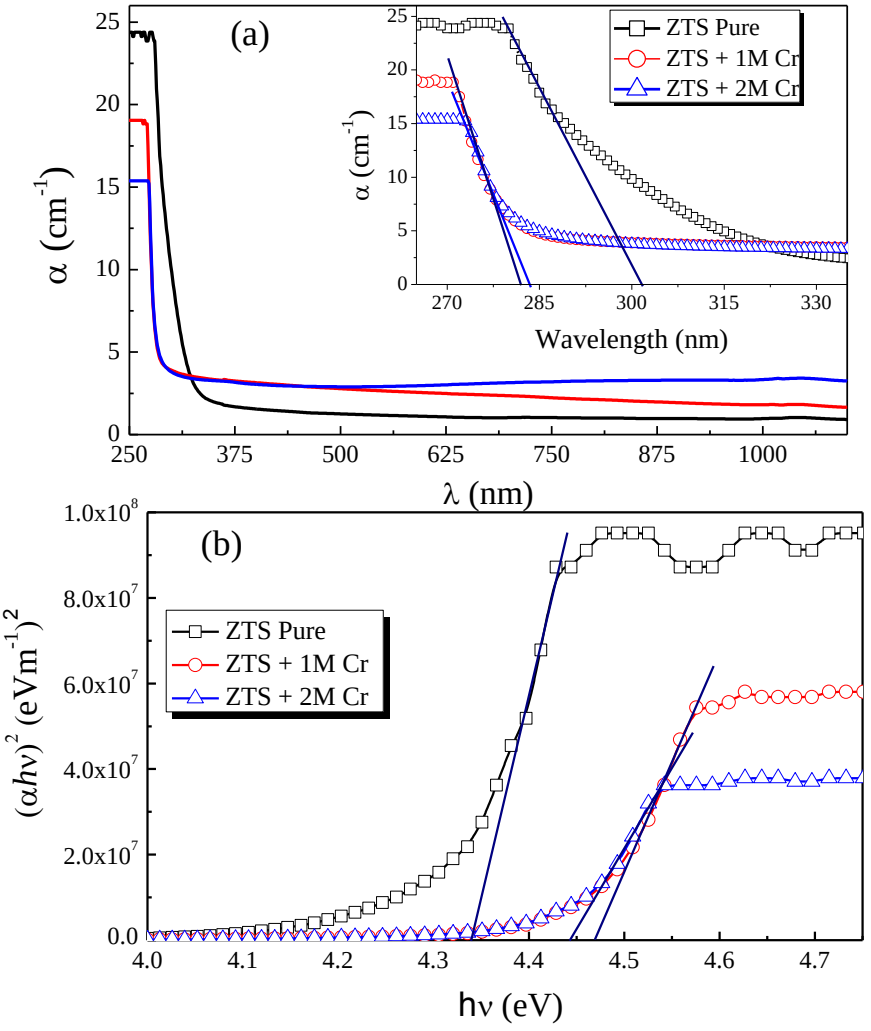

Fig. 8.7: *(a) the absorption spectra, the inset indicates blue shift of absorption edge. (b) shows the increase in band gap of doped single crystals*

The values of E_g for pure, 1 mol% and 2 mol% doped specimens are respectively 4.34, 4.47 and 4.44 eV. These results indicate that doping has increased E_g considerably. This behaviour of increase in the band gap is similar to that reported for reduced yttria-stabilized zirconia (PaiVerneker *et al.,* 1898). The widening of E_g for doped crystals indicates the absence of the localized states in the band gap which might have been present in pure crystal and obscure the true band gap. The localized states in the energy gap generally occur for the crystals having extrinsic defects or disorders (Stapper *et al.,* 1999). The slightly higher value for 1 mol% specimen in comparison with that of 2 mol% specimen may be attributed to the better perfection of former one. The blue shift as observed in §8.4.3 for the PL peak position may be attributed to the increase in the band gap energy due to doping.

8.4.5 Wavelength dispersion analysis

The measured refractive index (RI) and extinction coefficient are plotted as a function of wavelength. The room temperature linear RI dispersion spectra for pure and 1 mol% Cr^{3+} doped crystals are shown in Fig. 8.8(*a*). We could not get the values of refractive index for 2 mol% due to very low reflected intensity from the crystal surface having high absorbance as has been observed in UV-VIS analysis. The wavelength dependent theoretical refractive index values were calculated using the Sellmeier's equation:

$$n^2 = A + \frac{B}{\lambda^2 - C} - D\lambda^2 \tag{8.1}$$

where, *A, B, C,* and *D*, are the Sellmeier coefficients and the values of these are respectively 2.8437, 0.0372, 0.0333 and 0.009167 used from the literature (Marcy *et al.,* 1992). Wavelength, λ is taken in micrometer. The theoretical RI vs. λ plot (solid green line) is shown along with experimental RI plots for pure and Cr^{3+}-doped ZTS crystals. The experimental results of RI for both the crystals obtained from the ellipsometry analysis follow the same behaviour as that of theoretical one. However, in comparison to theoretical values, the pure crystal exhibits lower RI values in lower wavelength region and well matched for higher wavelengths. For the Cr^{3+} doped crystal, the RI values are well matched with theoretical values at lower wavelengths and at longer wavelengths region these are higher in comparison to those of pure

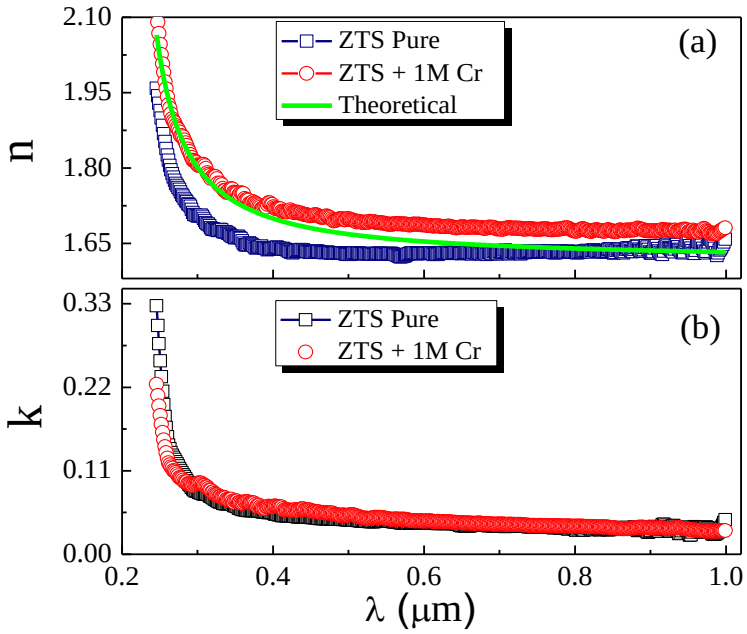

Fig. 8.8: *(a) The linear refractive index and (b) the extinction coefficient of pure and 1 mol% Cr-doped ZTS single crystals*

as well as theoretical. The theoretical as well as experimentally obtained refractive indices with wavelength are given in Table 8.1. The Cr^{3+} is photorefractive in nature and hence modifies the refractive index and other optical properties of host crystals by the electro-optic phenomenon significantly (Chah *et al.*, 1997; Deanna *et al.*, 1998).

The extinction coefficients (*k*) for pure and doped crystals are plotted with respect to wavelength in Fig. 8.8(*b*). Both the pure and doped crystals have similar *k* values over the entire wavelength range. The linear response of the system to electromagnetic radiation is described by the dielectric function (ε). The real (ε_r) and imaginary (ε_i) parts of optical dielectric constant of the ZTS single crystals are determined using the following relations given in equation (6.5) [§4.4.7].

The variations of real part ε_r and imaginary part ε_i are shown respectively in (a) and (b) of Fig. 8.9. Both ε_r and ε_i have higher values at lower wavelengths and decrease very fast with increase in wavelength but for the wavelengths above 400 nm these remain almost constant. The ε_r values for doped specimen are higher over the entire wavelength range. However ε_i values are almost same for both the crystals. The higher values of ε_r are due to Cr^{3+} doping. The dielectric constant is directly proportional to the polarizability of the crystal and the polarizability is to be

Table 8.1: *The theoretically calculated and experimentally obtained linear refractive indices of ZTS single crystals*

	Refractive index		
λ (μm)	ZTS Pure	ZTS + 1 mol% Cr	ZTS theoretical
0.245	1.9585	2.0650	2.1144
0.250	1.9140	2.0171	2.0462
0.300	1.7040	1.8011	1.8063
0.351	1.6612	1.7313	1.7504
0.400	1.6403	1.6990	1.7229
0.450	1.6321	1.6803	1.7048
0.501	1.6278	1.6679	1.6986
0.550	1.6284	1.6597	1.6887
0.601	1.6300	1.6534	1.6866
0.650	1.6296	1.6488	1.6821
0.701	1.6338	1.6451	1.6782
0.750	1.6326	1.6422	1.6778
0.801	1.6320	1.6397	1.6735
0.850	1.6320	1.6376	1.6737
0.900	1.6301	1.6357	1.6754
0.950	1.6301	1.6341	1.6731
1.000	1.6300	1.6326	1.6810

connected with valance charge density. The doped Cr^{3+} ions contribute significantly to the polarizability and hence lead to the higher values of ε_r (David *et al.*, 2009).

The dispersion plays an important role in the research for optical materials due a significant factor in optical communication and in designing the devices for spectral dispersion. The single-oscillator parameters were calculated and analyzed using Wemple-DiDomenico model (DiDomenico *et al.*, 1969) [§4.4.7]. The E_o and E_d parameters for pure as well as doped ZTS crystals have been obtained by plotting $1/(n^2\text{-}1)$ *vs.* $(h\nu)^2$ in Fig. 8.10 for the 3-12 $(eV)^2$ range of $(h\nu)^2$. The plot for the doped crystal indicates higher slope compared to that of pure. The solid dark yellow and violet lines are fitted linearly with the data points for pure and doped crystals respectively. The E_o and E_d have been calculated from the slope $(E_oE_d)^{-1}$ and intercept the (E_o/E_d) of the linearly fit curves in the given energy range and their values are given in Table 8.2. The oscillator strength and dispersion energies of crystals strongly depend on their structures (Wemple & DiDomenico, 1969). The ZTS crystals belong to the space group $Pca2_1$ with $Z = 4$ (Oussaid *et al.* 2000). The Zn^{2+} ions are tetrahedrally coordinated with three sulphur atoms of thiourea and one sulphate oxygen where all three thiourea molecules are nearly coplanar and the

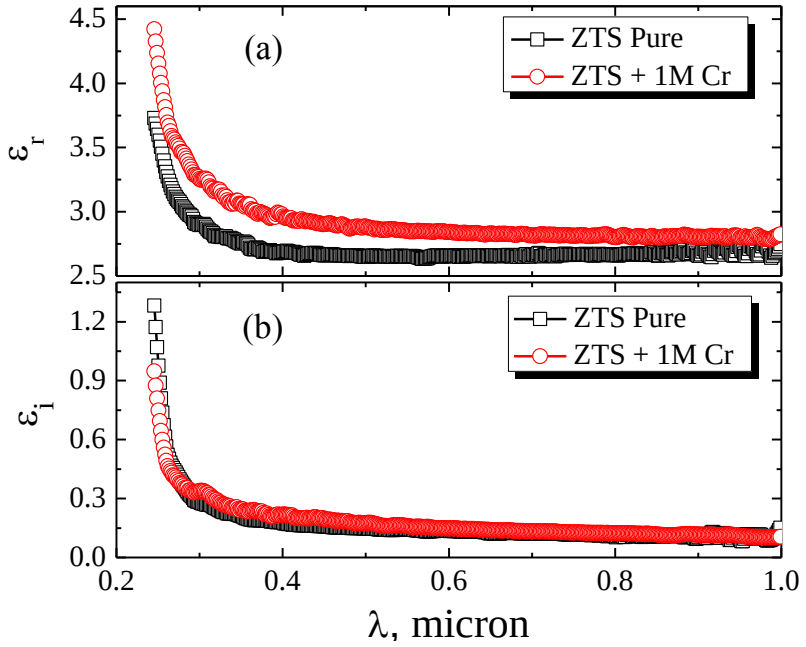

Fig. 8.9: *(a) Real and (b) imaginary optical dielectric constants of pure and 1 mol% Cr-doped ZTS single crystals*

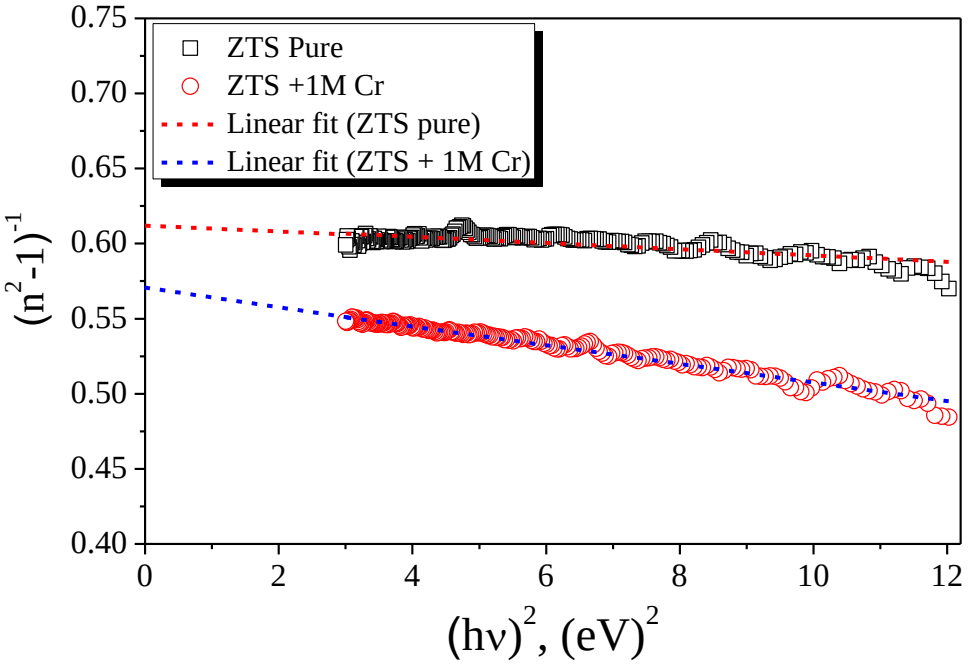

Fig. 8.10: *The $(n^2 – 1)^{-1}$ vs. $h\nu^2$ plots for pure and 1 mol% doped ZTS single crystals. The dashed straight lines are the linear fit of the data points*

sulphur atoms of thiourea molecule are equidistant from Zn (Venkataramanan *et al.* 1994). The evaluated E_o and E_d parameters for ZTS fall in the category of tetrahedrally coordinated systems (Wemple & DiDomenico, 1971). The observed

Table 8.2: *The E_o and E_d parameters for pure and Cr doped ZTS single crystals*

Crystal	E_0 (eV)	E_d (eV)
ZTS Pure	17.505	28.563
ZTS + 1M Cr	9.723	17.072

lower values of E_o and E_d due to Cr-doping may be attributed to Cr^{3+} ions in the lattice of ZTS which cause the redistribution of electronic charge around these ions and lead to the modification of the spectroscopic properties of the crystals (Ramirez *et al.*2004; Ramirez *et al.*2005) and hence the refractive index by the process of photorefraction (Kushwaha *et al.*, 2011).

8.5 CONCLUSION

Pure and chromium doped single crystals of ZTS have been successfully grown by SEST method. The actual concentration of chromium incorporated into the grown doped crystals found to be very less i.e. 45 and 55 ppm compared to that of 1.0 and 2.0 mol%, added into the solutions for doping during the crystal growth. The crystal structure and space group of the grown crystals were confirmed with the help of powder X-ray diffraction. The HRXRD analysis revealed that the grown crystals are almost perfect and the incorporated chromium is properly accommodated into the crystalline lattice without leading to the formation of any major defects like structural grain boundaries. From HRXRD analysis it is inferred that the doped Cr^{3+} ions lead to the creation of vacancy defects in the lattice to maintain the charge neutrality of the crystals. The anomalously enhanced PL emission intensity at higher doping level also demonstrates the formation of vacancies (F-centres), well in tune with the HRXRD analysis. For doped crystals the UV-VIS optical transparency of the crystals successively reduced with the concentration of Cr^{3+}. However, a large blue shift in cut off wavelength was taken place and the band gap increased from 4.34 eV to 4.47 and 4.44 eV for 45 and 55 ppm incorporation of Cr^{3+} in the matrix of crystal lattice. The linear refractive index, extinction coefficient and the real and imaginary optical dielectric constants for pure and 1 mol% doped crystals have been evaluated. The chromium doping in ZTS crystal leads to the enhancement of refractive index and makes its suitability for the photorefractive applications.